Dipole strength distribution in ^{206}Pb for the evaluation of the neutron capture cross section of ^{205}Pb

T. Shizuma,[1,2] N. Iwamoto,[2] A. Makinaga,[3,4] R. Massarczyk,[5] R. Schwengner,[6] R. Beyer,[6] D. Bemmerer,[6] M. Dietz,[6] A. Junghans,[6] T. Kögler,[6] F. Ludwig,[6] S. Reinicke,[6] S. Schulz,[6] S. Urlaß,[6] and A. Wagner[6]

[1]*National Institutes for Quantum and Radiological Science and Technology, Tokai, Ibaraki 319-1106, Japan*
[2]*Japan Atomic Energy Agency, Tokai, Ibaraki 319-1195, Japan*
[3]*Graduate School of Medicine, Hokkaido University, Sapporo 060-8638, Japan*
[4]*JEIN Institute for Fundamental Science, Kyoto 606-8317, Japan*
[5]*Los Alamos National Laboratory, Los Alamos, New Mexico 87545, USA*
[6]*Helmholtz-Zentrum Dresden-Rossendorf, Dresden 01328, Germany*

(Received 26 October 2017; revised manuscript received 16 October 2018; published 19 December 2018)

The dipole strength distribution of ^{206}Pb was investigated via a nuclear resonance fluorescence experiment using bremsstrahlung produced with an electron beam at a kinetic energy of 10.5 MeV at the linear accelerator ELBE. We identified 88 states resonantly excited at energies from 3.7 to 8.2 MeV. The analysis of the measured γ-ray spectra includes the quasicontinuum of levels at high energy. Monte Carlo simulation of γ-ray cascades were performed to obtain the intensities of inelastic transitions and branching ratios of the ground-state transitions. The extracted photoabsorption cross section shows enhanced dipole strength at the excitation energies around 5.5 and 7 MeV, which may related to a pygmy dipole resonance. The present (γ, γ') data combined with (γ, n) data from the literature were used for confining input parameters of the statistical calculation code CCONE to derive the neutron-capture cross section of the unstable ^{205}Pb nucleus.

DOI: 10.1103/PhysRevC.98.064317

I. INTRODUCTION

Photon strength functions (PSFs) have attracted growing interest in the context of nuclear astrophysics [1] and nuclear technologies [2,3]. They give information on average electromagnetic decay properties of the nucleus and are dominated by the electric giant dipole resonance (GDR). However, the dipole strength distribution close to the neutron separation energy has a large impact on the neutron-capture cross sections [4,5]. The PSFs are essential ingredients of statistical nuclear reaction calculations to estimate cross sections of nuclear reactions, for example, neutron capture.

From the viewpoint of nuclear engineering, cross-section data of capture reactions induced by fast neutrons are crucial for the development of the transmutation technique through accelerator driven systems (ADS) [6]. In particular, there is a need of the cross-section data with high accuracy for plutonium and minor actinides. In addition, reliable cross sections of fast neutron-capture reactions for lead and bismuth are required because these materials are used as a spallation target and a coolant in the ADS [7]. Among lead isotopes, the unstable ^{205}Pb nucleus with a half-life of 1.73×10^7 years is of special interest, because this nucleus is produced by the neutron-capture reaction on ^{204}Pb and behaves like a stable isotope in the system. The accumulated amount of ^{205}Pb also has to be evaluated because it has long-lasting radiotoxicity.

Neutron-capture cross sections of ^{205}Pb have been measured using thermal neutrons from the Oak Ridge High Flux Isotope Reactor [8]. However, no experimental data of capture cross sections at the fast-neutron energy region are available. To evaluate the neutron-capture cross sections of ^{205}Pb, nuclear photon-scattering or nuclear resonance fluorescence (NRF) data combined with the photoneutron (γ, n) data can be used [9–11].

In the present work, the dipole strength of ^{206}Pb was measured in an NRF experiment. As the NRF occurs only via electromagnetic interactions, the transition strength can be extracted from the measured scattering intensities in a model-independent fashion [12]. In addition, predominantly, $J = 1$ states and, to lesser extent, $J = 2$ states are excited from the ground state in an even-even nucleus. The present NRF experiment aims at the determination of the photoabsorption cross section and the dipole strength functions based on the measured scattering cross sections. The neutron-capture cross sections of ^{205}Pb will be determined by constraining the statistical model parameters, especially the PSFs, based on the experimental data.

II. EXPERIMENTAL PROCEDURE

The present NRF experiment on ^{206}Pb was performed at the bremsstrahlung facility γELBE [13] of the Helmholtz-Zentrum Dresden-Rossendorf (HZDR). Bremsstrahlung was produced using an electron beam at a kinetic energy of 10.5 MeV with an average beam current of 470 μA at a micropulse repetition rate of 13 MHz. The electron beam hit a radiator consisting of a niobium foil with a thickness of 5 μm. The electron energy was chosen as the flux was sufficiently high up to the neutron separation energy $S_n =$ 8.0881 MeV. The bremsstrahlung was collimated by an Al collimator with a length of 2.6 m and an opening angle of 5 mrad. A cylindrical Al absorber with a length of 10 cm was

 ©2018 American Physical Society

placed between the radiator and the collimator to reduce the low-energy bremsstrahlung.

The target consisted of two disks of ^{206}Pb with a diameter of 20 mm tilted by 45° about a vertical axis perpendicular to the beam. The target mass was 3940 mg, enriched to 99.3% in ^{206}Pb. The lead disks were combined with 400 mg of boron, enriched to 99.5% in ^{11}B, that was also shaped to a disk of 20 mm diameter to determine the photon flux from known scattering cross sections of levels in ^{11}B.

Scattered photons were measured with four high-purity germanium (HPGe) detectors with relative efficiencies of 100% and 60%. All HPGe detectors were surrounded by escape-suppression shields made of bismuth germanate scintillation detectors. Two HPGe detectors with relative efficiencies of 60% were placed horizontally at 90° relative to the photon beam direction at a distance of 28 cm from the target. The other two HPGe detectors with relative efficiencies of 100% were placed vertically at 127° to the beam at a distance of 32 cm from the target. The ratios of the γ-ray intensities measured at 90° and 127° are used to distinguish between dipole and quadrupole radiation. To reduce the contribution of low-energy photons, absorbers of 8-mm Pb plus 3-mm Cu were placed in front of the detectors at 90°, and 3-mm Pb plus 3-mm Cu were used for the detectors at 127°. Spectra of scattered photons were measured for 126 h. Further details of the measurement techniques are given in Refs. [14,15].

III. RESULTS

A. Integrated scattering cross section

Part of a spectrum including events measured with the two detectors at 127° relative to the beam is shown in Fig. 1. In photon-scattering experiments the energy-integrated scattering cross section I_s of an excited state at the energy of E_x can be deduced from the measured intensity of the respective transitions to the ground state. It can be determined relative to the known integrated scattering cross sections $I_s(E_x^B)$ of states

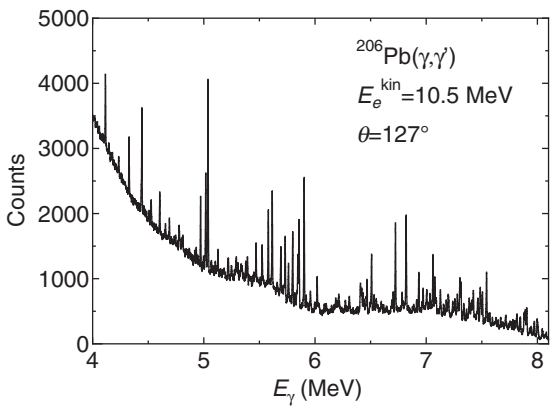

FIG. 1. Part of a spectrum of photons scattered from ^{206}Pb combined with ^{11}B, measured during the irradiation with bremsstrahlung produced by electrons at the kinetic energy of 10.5 MeV. This spectrum is the sum of the spectra measured with the two detectors at 127° relative to the beam.

in ^{11}B [16]:

$$\frac{I_s(E_x)}{I_s\left(E_x^B\right)} = \left[\frac{I_\gamma(E_\gamma,\theta)}{W(E_\gamma,\theta)\Phi_\gamma(E_x)N_N\lambda}\right] \times \left[\frac{I_\gamma\left(E_\gamma^B,\theta\right)}{W\left(E_\gamma^B,\theta\right)\Phi_\gamma\left(E_x^B\right)N_N^B\lambda^B}\right]^{-1}.$$

Here $I_\gamma(E_\gamma,\theta)$ and $I_\gamma(E_\gamma^B,\theta)$ denote efficiency-corrected intensities of a ground-state transition at E_γ and of a ground-state transition in ^{11}B at E_γ^B, respectively, observed at a scattering angle θ to the beam. $W(E_\gamma,\theta)$ and $W(E_\gamma^B,\theta)$ represent the angular correlations of these transitions. The quantities $\Phi(E_x)$ and $\Phi_\gamma(E_x^B)$ are the photon fluxes at the energy of the considered level and at the energy of a level in ^{11}B, respectively. The quantities N_N and N_N^B stand for the numbers of nuclei in the ^{206}Pb and ^{11}B targets, respectively. The quantities λ and λ^B are the correction factors of atomic and self-absorption for the levels at E_x in ^{206}Pb and at E_x^B in ^{11}B, respectively. These correction factors were determined according to Eq. (19) in Ref. [17]. The determination of the integrated cross sections relative to the ones of states in ^{11}B has the advantage that the efficiencies of the detectors and the photon flux are needed in relative units only. We calculated the energy-dependent efficiencies for the four HPGe detectors by using GEANT4 [18]. The simulated efficiency curves were checked by using efficiencies measured with a ^{226}Ra calibration source. The bremsstrahlung spectrum was calculated by using a code [19] based on the approximation given in Ref. [20] and including a screening correction according to Ref. [21]. The calculated curve of the photon flux fits the experimental value derived from measured intensities, known integrated cross sections [16] and angular distributions [22] of transitions in ^{11}B.

The integrated scattering cross section I_s is related to the partial decay width Γ_0 to the ground state and the total decay width Γ according to

$$I_s = \int \sigma_{\gamma\gamma} dE = \frac{2J_x+1}{2J_0+1}\left(\frac{\pi\hbar c}{E_x}\right)^2 \frac{\Gamma_0^2}{\Gamma}, \qquad (1)$$

where $\sigma_{\gamma\gamma}$ is the elastic-scattering cross section and J_0 and J_x denote the spins of the ground state and the excited state, respectively.

Spins of the excited states were deduced by comparing the ratios of γ-ray intensities measured with the HPGe detectors at two different angles with theoretical predications. The optimum combination is angles of 90° and 127° because the ratios for the respective spin sequences $0-1-0$ and $0-2-0$ differ most at these angles. The expected values are $W(90°)/W(127°)_{0-1-0} = 0.74$ and $W(90°)/W(127°)_{0-2-0} = 2.18$, taking into account the finite solid angle of the detectors.

The deduced values for excitation energies, angular distribution ratios, spin assignments, the ratios Γ_0^2/Γ, and branching ratios into the ground state are listed in Table I. Figure 2 shows the integrated cross sections deduced from the present experimental data. We observed 85 states with $J = 1$ and 3 states with $J = 2$ below the neutron separation energy, including 33 states newly identified. A comparison of the Γ_0^2/Γ

TABLE I. Results of the ^{206}Pb(γ, γ') measurements. The excitation energies E_x, the angular distribution ratios $W(90°)/W(127°)$, the spin assignments J, the ratios Γ_0^2/Γ, and the branching ratios Γ_0/Γ are given. The values of Γ_0^2/Γ known from previous measurements are also listed for comparison.

E_x[a] (keV)	$W(90°)/W(127°)$	J	Γ_0^2/Γ[b] (eV)	Γ_0/Γ	Γ_0^2/Γ[c] (eV)	Γ_0^2/Γ[d] (eV)	Γ_0^2/Γ[e] (eV)	Γ_0^2/Γ[f] (eV)
3742.7(2)	0.35(14)	1	0.13(2)	1.0	0.09(1)			
4115.2(1)	2.09(20)	2	0.21(2)	1.0	0.29(3)	0.58(15)		0.30(6)
4146.1(7)	1.3(3)	1	0.05(2)	1.0	0.03(2)			
4328.0(1)	0.66(11)	1	0.33(3)	1.0	0.33(4)	0.48(11)		0.90(9)
4603.8(1)	0.63(15)	1	0.30(3)	1.0	0.25(3)	0.58(16)		0.23(3)
4690.7(2)	0.8(3)	1	0.13(2)	1.0	0.08(2)			
4778.2(5)[g]	0.83(11)	1	0.48(12)	0.85(6)	0.20(14)			
4805.2(3)	0.8(4)	1	0.06(1)	1.0				
4932.6(3)	3.0(9)	2	0.07(1)	1.0	0.04(1)			
4971.1(1)	0.93(15)	1	0.71(5)	1.0	0.7(7)	0.95(23)	0.8(3)	0.8(2)
5037.8(1)	0.79(7)	1	2.33(16)	0.92(5)	2.12(21)	2.6(4)	1.6(6)	2.3(5)
5127.6(2)	0.86(19)	1	0.23(3)	1.0	0.23(3)			
5377.2(3)	0.92(21)	1	0.23(5)	1.0	0.28(4)			
5459.0(5)	0.61(23)	1	0.14(3)	0.48(10)	0.09(2)			
5470.2(1)	0.82(12)	1	0.49(4)	1.0	0.58(7)	0.7(2)		
5524.5(2)	0.88(11)	1	0.56(6)	1.0	0.4(5)			
5579.9(1)	0.87(9)	1	1.23(9)	1.0[h]	1.47(17)	1.7(3)	0.5[i]	
5615.2(1)	0.81(7)	1	1.77(12)	0.91(5)	2.02(23)	1.8(4)	1.0[i]	
5692.9(1)	0.81(11)	1	0.88(7)	1.0	0.95(14)	0.8(2)	0.5[i]	
5721.7(6)	0.71(24)	1	0.19(5)	0.57(8)	0.19(3)			
5732.0(1)	0.70(7)	1	0.99(12)	1.0	1.44(32)	1.3(3)		
5761.3(1)	0.73(12)	1	0.72(6)	1.0	0.68(9)	0.9(2)		
5799.3(1)	0.86(9)	1	2.16(16)	1.0	1.68(20)	1.1(3)	1.0[i]	
5818.3(3)	0.84(24)	1	0.18(4)	1.0	0.25(4)	0.5(2)		
5845.8(1)	0.89(10)	1	0.99(8)	1.0	1.15(21)	1.1(2)	3.0[i]	
5857.0(1)	0.85(8)	1	1.79(13)	1.0	2.17(27)	2.0(4)		
5902.4(1)	0.77(6)	1	2.88(20)	1.0	3.48(44)	3.0(6)	4.4(18)	
5951.4(6)	0.54(24)	1	0.13(5)	1.0	0.13(5)			
5959.4(6)	1.06(11)	1	0.53(14)	1.0	0.34(6)			
5999.4(6)	1.00(16)	1	0.18(4)	1.0	0.09(5)			
6019.7(2)	1.07(14)	1	0.73(6)	1.0	0.66(9)			
6100.3(6)	1.33(16)	1	0.24(5)	1.0	0.32(7)			
6149.1(5)	0.7(3)	1	0.16(4)	1.0				
6185.8(6)	2.1(5)	2	0.16(2)	1.0				
6200.0(8)	1.1(4)	1	0.20(5)	1.0	0.21(4)			
6409.1(2)	0.86(11)	1	0.96(9)	1.0	0.65(15)			
6419.8(2)	0.89(13)	1	0.82(7)	1.0	0.4(10)			
6432.5(3)	0.98(18)	1	0.58(6)	1.0	0.35(10)			
6442.6(5)	0.79(22)	1	0.38(5)	1.0	0.22(9)			
6458.8(6)	0.55(14)	1	0.36(8)	1.0				
6467.8(2)	0.84(12)	1	0.76(9)	0.83(5)	0.46(42)			
6508.6(1)	0.87(11)	1	1.79(14)	1.0	0.24(20)	1.9(4)		
6531.3(2)	0.91(16)	1	0.34(5)	1.0				
6691.9(3)	1.15(25)	1	0.37(5)	1.0				
6723.5(1)	0.78(7)	1	3.12(22)	0.86(5)		3.4(6)	5.5(22)	
6819.7(1)	0.75(6)	1	3.88(27)	1.0		4.7(9)	7.4(30)	
6933.8(1)	0.73(9)	1	1.65(13)	1.0				
7061.5(1)	0.76(10)	1	3.14(27)	1.0		2.5(6)		
7077.6(2)[j]	0.63(11)	1	1.83(19)	0.74(6)		0.9(3)		
7128.2(2)	0.89(15)	1	1.20(12)	1.0		1.0(2)		
7158.5(5)	0.88(20)	1	0.79(11)	1.0				
7181.1(4)	0.72(14)	1	0.85(10)	1.0				
7199.8(3)	0.67(10)	1	1.61(15)	1.0				
7238.7(6)	0.71(22)	1	0.57(10)	1.0				

TABLE I. (*Continued.*)

E_x[a]	$W(90^\circ)/W(127^\circ)$	J	Γ_0^2/Γ[b]	Γ_0/Γ	Γ_0^2/Γ[c]	Γ_0^2/Γ[d]	Γ_0^2/Γ[e]	Γ_0^2/Γ[f]
7258.6(4)	0.85(17)	1	0.90(11)	1.0				
7302.6(3)	0.79(12)	1	1.90(18)	1.0				
7312.6(3)	0.76(12)	1	1.89(18)	1.0				
7338.2(7)	0.9(4)	1	1.06(42)	1.0				
7362.9(3)	0.62(18)	1	0.52(9)	1.0				
7387.5(2)	0.97(16)	1	0.87(9)	1.0				
7404.5(3)	0.92(17)	1	0.61(7)	1.0				
7414.1(3)	0.83(14)	1	0.79(8)	1.0				
7424.1(2)	1.07(13)	1	1.32(12)	1.0		1.6(4)		
7464.8(5)	0.8(5)	1	2.19(53)	1.0		0.9(4)		
7486.1(2)	0.93(12)	1	1.91(17)	1.0		1.7(4)		
7493.5(3)	0.79(13)	1	1.19(12)	1.0				
7505.9(1)	0.68(9)	1	2.00(16)	0.66(4)		1.2(4)		
7542.9(1)	0.86(8)	1	3.28(24)	1.0		2.3(6)		
7556.4(4)	0.79(25)	1	0.48(7)	1.0				
7571.4(3)	0.91(14)	1	0.65(9)	1.0		1.1(5)		
7597.3(14)	0.91(21)	1	0.27(8)	1.0				
7627.6(5)	0.88(13)	1	0.53(13)	1.0				
7645.9(3)	0.66(18)	1	0.31(7)	1.0				
7669.7(3)	0.7(3)	1	0.50(9)	1.0				
7715.5(4)	0.68(19)	1	1.10(16)	1.0				
7781.1(3)	0.61(12)	1	0.68(12)	1.0				
7798.4(7)	0.59(12)	1	0.58(13)	1.0				
7815.4(3)	0.79(9)	1	1.60(20)	0.87(5)		0.8(2)		
7845.5(3)	0.84(28)	1	1.83(22)	0.71(7)		1.9(4)		
7881.1(3)	0.87(10)	1	1.46(13)	1.0[k]		1.1(3)		
7891.2(2)	0.76(8)	1	1.95(16)	0.55(4)		1.6(4)		
7904.3(2)	0.74(8)	1	2.47(20)	0.70(4)		2.2(5)		
7930.3(7)	1.0(3)	1	0.43(11)	1.0				
7944.7(4)	0.89(17)	1	0.75(12)	1.0				
8001.6(3)	0.74(10)	1	2.64(30)	1.0		1.6(4)		
8046.5(4)	0.87(8)	1	0.79(17)	1.0				
8079.8(7)	0.88(11)	1	0.41(9)	1.0				
8118.5(4)	0.82(10)	1	0.37(8)	1.0				

[a]The peak fitting error in parenthesis is given in units of the last digit. This energy was deduced from the γ-ray energy measured at 127° to the beam.
[b]This work. The statistical and systematic uncertainties (associated with strength normalization, photon flux, and efficiency) are reflected in the errors.
[c]Values taken from Ref. [26].
[d]Values taken from Ref. [25].
[e]Values taken from Ref. [24].
[f]Values taken from Ref. [23].
[g]Transition into the ground state coincides with a possible branch of the state at 5580 keV.
[h]Possible branch to the 2_1^+ state coincides with the transition at 4778 keV.
[i]Estimated uncertainty in excess of 50%.
[j]Transition into the ground state coincides with a possible branch of the state at 7881 keV.
[k]Possible branch to the 2_1^+ state coincides with the transition at 7078 keV.

ratios obtained in the present experiment with previous work [23–26] is also shown in Table I. The present results are generally in good agreement with those previously published. Spins for excited states at 4932.6, 5459.0, 5951.4, and 5999.4 keV were newly determined in this work based on the angular distribution ratios. The present spin assignment for the 6100.3-keV level is not consistent with the previous work using inelastic electron scattering [27]. Previously reported resonance states at 4483.5, 5408.4, and 6110.7 keV [26] could not be confirmed, but their transition strengths are around the present detection limit. The total dipole strength in the energy region from 4.9 to 8.1 MeV is also consistent with the data recently published [28].

B. Determination of the photoabsorption cross section

The determination of the absorption cross section required a correction to the experimental spectrum for detector

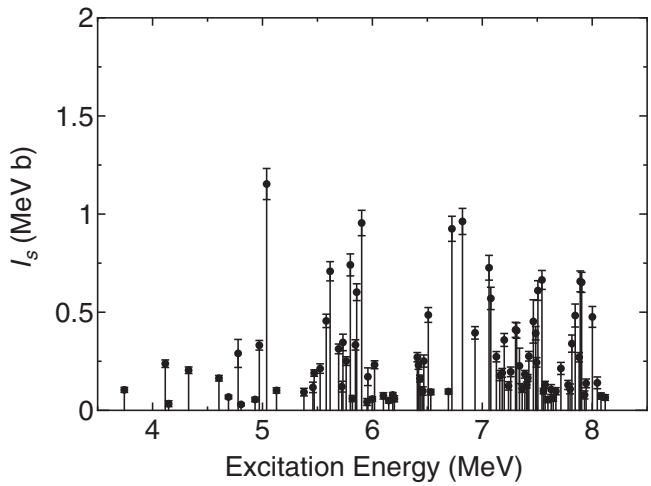

FIG. 2. Integrated scattering cross sections deduced from the present experiment.

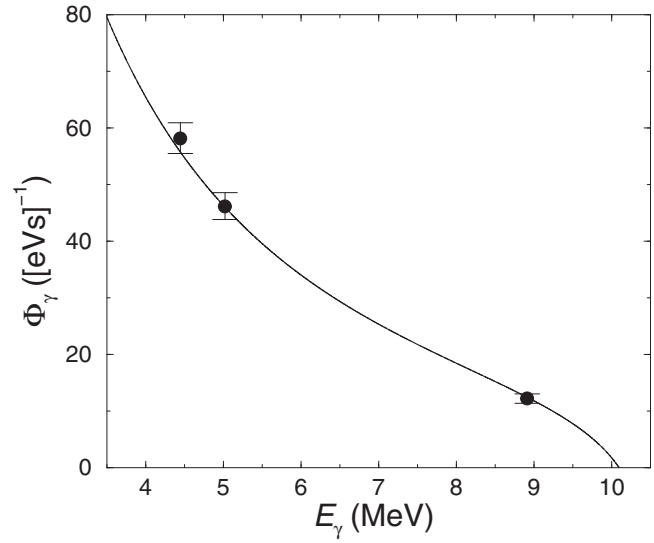

FIG. 3. Absolute photon flux at the target deduced from intensities of known transitions in ^{11}B (circles) using the detector efficiency calculated with GEANT4 and the adjusted relative flux calculated as described in the text (solid line).

response, absolute efficiency and absolute photon flux due to atomic processes, such as Compton scattering and pair creation induced by the impinging photons in the target material, and for ambient background radiation. The detector response was simulated using the program package GEANT4 [18]. The reliability of the simulation was tested by comparing simulated spectra with measured ones as illustrated, for example, in Ref. [29].

The absolute efficiencies of the HPGe detectors in the setup at ELBE were determined experimentally up to 2.4 MeV from measurements with ^{137}Cs, ^{154}Eu, and ^{226}Ra calibration sources. For interpolation, an efficiency curve calculated with GEANT4 and scaled to the absolute experimental values was used. From the adjustment of the curve to the experimental values, an overall uncertainty of the absolute efficiency of 5% was deduced and used in the further analysis (cf. Ref. [29]). A check of the simulated efficiency curve at high energy up to about 9 MeV was performed via various (p,γ) reactions at the HZDR Tandetron accelerator. The efficiency values deduced from these measurements agreed with the simulated values within their uncertainties [30]. Similar results were obtained for the resonances at 4.44 and 11.66 MeV in ^{12}C populated in the ^{11}B(p,γ) reaction at the Triangle Universities Nuclear Laboratory Van-de-Graaff accelerator [31].

First, a spectrum of the ambient background adjusted to the intensities of the transitions from ^{40}K and ^{208}Tl decay in the in-beam spectrum was subtracted from the measured spectrum. To correct the spectrum for the detector response, spectra of monoenergetic γ rays were calculated in steps of 10 keV by using the simulation code GEANT4. Starting from the high-energy end of the experimental spectrum, the simulated spectra were subtracted sequentially (spectrum-strip method). The absolute photon flux was deduced from the intensities of the transitions in ^{11}B (cf. Fig. 3). The response-, efficiency-, and flux-corrected spectrum is shown in Fig. 4. The background produced by atomic processes in the ^{206}Pb target was obtained from a GEANT4 simulation. The corresponding spectrum of the atomic background is also displayed in Fig. 4.

As can be seen in Fig. 4, the spectrum of photons scattered from ^{206}Pb contains resolved peaks and a quasicontinuum that is considerably higher than the background caused by atomic-scattering processes. This continuum is formed by a number of nonresolved transitions of small intensities which are a consequence of the high nuclear level density at high energy in connection with the finite detector resolution. The relevant intensity of the photons resonantly scattered from ^{206}Pb is obtained from a subtraction of the atomic background from the response-corrected experimental spectrum.

To deduce the correct dipole-strength distribution, inelastic transitions have to be removed from the spectrum and the

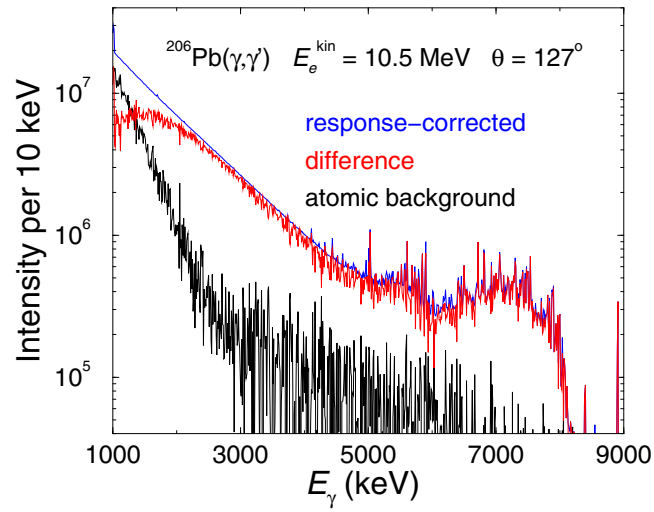

FIG. 4. Response-corrected spectrum of the two detectors placed at 127° (blue), simulated spectrum of photons scattered from the target to the detectors by atomic processes (black), and the difference of the two (red).

ground-state transitions have to be corrected for their branching ratios b_0. We applied statistical methods to estimate the intensities of branching transitions to low-lying excited levels and of the branching ratios of the ground-state transitions. These methods were also applied in earlier photon-scattering experiments at γELBE, for example, in Refs. [9,29,32–34].

The intensity distribution contains ground-state transitions and, in addition, branching transitions to lower-lying excited states (inelastic transitions) as well as transitions from those states to the ground state (cascade transitions). The different types of transitions cannot be clearly distinguished. However, for the determination of the photoabsorption cross section and the partial widths Γ_0 the intensities of the ground-state transitions are needed. Therefore, contributions of inelastic and cascade transitions have to be subtracted from the spectra. We corrected the intensity distributions by simulating γ-ray cascades from the levels in the whole energy range. The code γDEX [29,33,34] was used to do this. γDEX works analogously to the strategy of the code DICEBOX [35] developed for (n,γ) reactions, but in addition it includes also the excitation from the ground state. In these simulations, level schemes (nuclear realizations) including states with $J = 0,\ldots,5$ were created. We apply the statistical methods also for the low-energy part of the level scheme instead of using experimentally known low-lying levels, because this would require the knowledge of the partial decay widths of all transitions populating these fixed levels. Fluctuations of the partial widths were treated by applying the Porter-Thomas distribution [36].

Level densities were calculated by using the constant-temperature model [37] with the parameters $T = 0.78(5)$ MeV and $E_0 = 0.12(5)$ MeV adjusted to experimental level densities [38]. In the individual nuclear realizations, the values of T and E_0 were varied randomly within a Gaussian distribution with a σ corresponding to the uncertainties given in Ref. [38]. The parity distribution of the level densities was modeled according to the information given in Ref. [39].

The first input for the photon strength function simulations were assumed to be Lorentz-shaped. For the $E1$ strength a combination of three Lorentz functions, with parameters as described in Ref. [40], was used without deformation. The parameters for the $M1$ and $E2$ strengths were taken from global parametrizations of $M1$ spin-flip resonances and $E2$ isoscalar resonances, respectively [41].

Spectra of γ-ray cascades were generated for groups of levels in 100-keV bins. Starting from the high-energy end of the experimental spectrum, which contains ground-state transitions only, the simulated intensities of the ground-state transitions were normalized to the experimental ones in the considered bin. The intensity distribution of the branching transitions was subtracted from the experimental spectrum. Applying this procedure step by step for each energy bin moving toward the low-energy end of the spectrum, one obtains the intensity distribution of the ground-state transitions. Simultaneously, the branching ratios b_0^Δ of the ground-state transitions are deduced for each energy bin Δ. In an individual nuclear realization, the branching ratio b_0^Δ is calculated as the ratio of the sum of the intensities of the ground-state transitions from all levels in Δ to the total intensity of all transitions depopulating those levels to any low-lying levels including the ground state [9,10,29,32–34,42,43]. We obtain the absorption cross section in each bin as $\sigma_\gamma^\Delta = \sigma_{\gamma\gamma}^\Delta / b_0^\Delta$ for each nuclear realization by dividing the summed intensities in a bin of the experimental intensity distribution of the ground-state transitions with the corresponding branching ratio. Finally, the absorption cross sections of each bin were obtained by averaging over the values of the nuclear realizations. For the uncertainty of the absorption cross section a 1σ deviation from the mean has been taken.

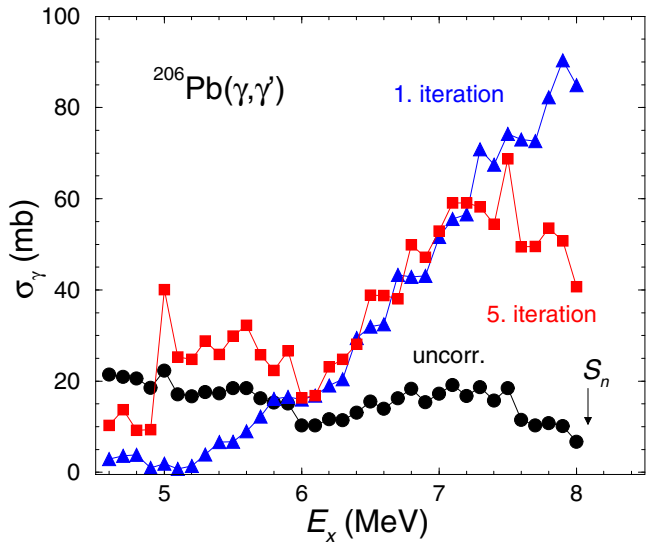

FIG. 5. Uncorrected photoabsorption cross section (black circles), and outputs of the first iteration step (blue triangles) and of the fifth (last) iteration step (red squares) in the simulation of γ-ray cascades.

The simulations were performed iteratively. The strength function obtained from an iteration step was used as the input for the next step. The iteration was stopped when the input strength function and the output strength function were in agreement within their uncertainties. Toward low energy, the uncertainties increase due to the use of the spectrum-strip method and the cross sections do not converge. Therefore, cross sections are not given below an excitation energy of 4.5 MeV. In Fig. 5, the input cross sections and the ones obtained from the first and last iteration steps are shown. The cross section obtained in the last iteration step is taken as the final absorption cross section. The uncertainties of the cross-section values include statistical uncertainties of the spectrum, the given uncertainty of the efficiency, uncertainties of the flux resulting from the integrated cross sections of the ^{11}B levels and the mentioned uncertainties of the level-density parameters.

IV. DISCUSSION

A. Photoabsorption cross section of ^{206}Pb

The absorption cross section of ^{206}Pb obtained from the procedure just described is shown in Fig. 6 together with the (γ,n) data of Ref. [44]. There are four values below

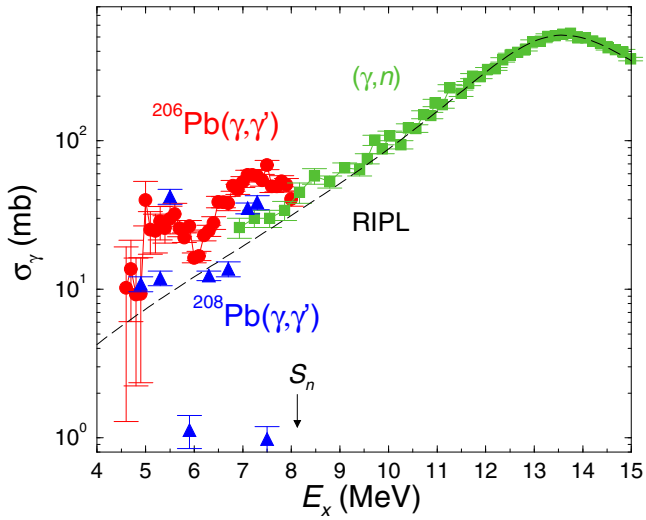

FIG. 6. Photoabsorption cross section of ^{206}Pb resulting from the present (γ, γ') experiment in connection with the techniques described in the text (red circles) and (γ, n) data of ^{206}Pb [44] (green squares). For comparison, the absorption cross section deduced from (γ, γ') data for ^{208}Pb [45] are shown (blue triangles). Also shown is the Lorentz curve from RIPL (black dashed line).

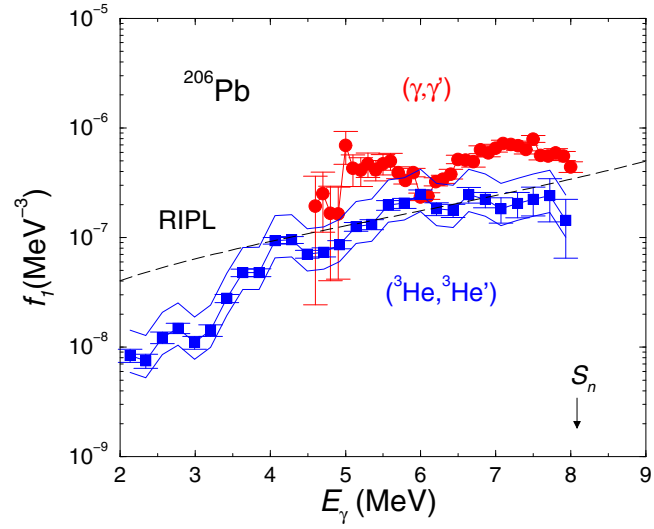

FIG. 7. Dipole strength functions for ^{206}Pb deduced from the present (γ, γ') data (red circles) and from $(^3\mathrm{He}, ^3\mathrm{He}')$ data (blue squares) [48]. The blue solid lines represent values based on lower and upper limits for the normalization of the $(^3\mathrm{He}, ^3\mathrm{He}')$ data. Also shown is the Lorentz curve with parameters taken from the RIPL database (black dashed line).

the neutron-separation energy, which is physically incorrect. For comparison, the absorption cross section deduced from (γ, γ') data for ^{208}Pb in an earlier study [45] is also shown. Note that the data of ^{208}Pb include resolved peaks only. The contribution of strength to the quasicontinuum was assumed to be small because of the small level density in the doubly magic ^{208}Pb and was neglected in the analysis [45]. The comparison shows that the cross-section values in ^{208}Pb in average amount to about 60% of that in ^{206}Pb. This behavior differs from that found in the series of xenon isotopes, in which the summed dipole strength in the energy region from 6 to 9 MeV increases with the neutron number [34]. Possible reasons are that the strength in the quasicontinuum may not be neglected in ^{208}Pb either or that there are structural differences that interfere the effect of the neutron excess. One observes a similarity in the shapes of the cross sections of ^{206}Pb and ^{208}Pb. Both nuclides show humps around about 5.5 and 7 MeV with a drop in between. This behavior reflects structural similarities of the two nuclei. It is correlated with the large widths of single levels (cf. Table I) that dominate the shape of the cross section over the quasicontinuum created by many weak level widths in nuclides around closed shells. Such a feature was also found in the $N = 50$ isotones ^{86}Kr [43], ^{88}Sr [14], and ^{90}Zr [46].

Strength-function data for ^{206}Pb are also available from $(^3\mathrm{He}, ^3\mathrm{He}')$ experiments. The strength function deduced from these experiments is compared with the dipole-strength function calculated from the present cross section for ^{206}Pb in Fig. 7. The shown $(^3\mathrm{He}, ^3\mathrm{He}')$ data result from a new reanalysis of the data in Ref. [47], which is based on updated response functions for the CACTUS detector array and an improved error estimate in the simultaneous extraction of level density and γ-ray strength from the primary γ-ray spectra [48]. Furthermore, the γ-ray strength was normalized to recent (γ, n) data [49] and also compared to the data in Refs. [44,50]. The systematic error in the absolute value of the order of 50% is not included in the displayed error bars. Also shown in Fig. 7 is a Lorentz curve with parameters adjusted to (γ, n) data and taken from the database Reference Input Parameter Library (RIPL) [41]. One sees that the two humps formed by the present data for ^{206}Pb represent extra strength above the RIPL curve. This can be considered as the pygmy dipole resonance. The two humps around 5.5 and 7 MeV exceed also the $(^3\mathrm{He}, ^3\mathrm{He}')$ data by a factor of up to three at their maxima. The deviation between the two data sets could partly be due to the uncertain absolute normalization of the $(^3\mathrm{He}, ^3\mathrm{He}')$ data. Besides, the $(^3\mathrm{He}, ^3\mathrm{He}')$ reaction populates states in a broad spin range up to $J \approx 12$. Transitions from 1^- states to the ground state are less dominant in this case, because they are included in an average together with many weak transitions from initial states of various spins.

For the neighboring isotope ^{208}Pb, the (γ, γ') data [45] can also be compared with reanalyzed $(^3\mathrm{He}, ^3\mathrm{He}')$ data [48] and, in addition, with results of a (p, p') experiment [51]. The respective strength functions are shown in Fig. 8. The (p, p') data also show peaks around 5.5 and 7 MeV with a drop in between as seen in the (γ, γ') data. Close to the neutron threshold, the ^{208}Pb(γ, γ') data are roughly compatible with both the $(^3\mathrm{He}, ^3\mathrm{He}')$ as well as the (p, p') data. At the neutron-separation energy S_n the (p, p') data increase further, whereas the (γ, γ') data drop because of the opening of the (γ, n) channel.

The relation between the strength functions from excitation $[(\gamma, \gamma')$ and $(p, p')]$ and deexcitation $[(^3\mathrm{He}, ^3\mathrm{He}')]$ may serve as a measure for the validity of the Brink-Axel hypothesis [52]. As just mentioned, differences between the (γ, γ') and

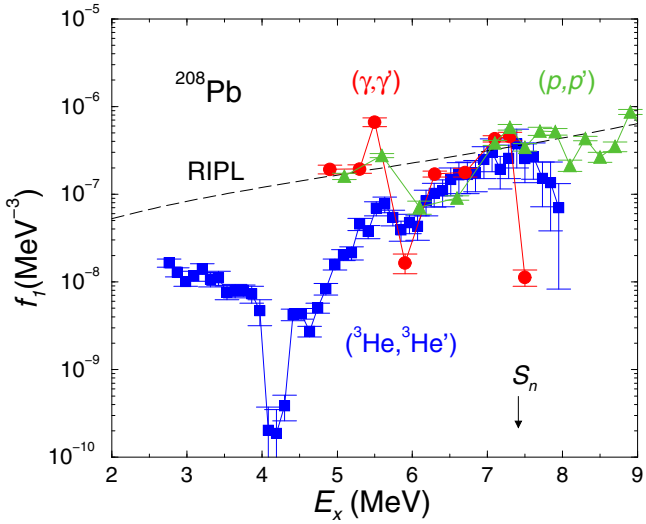

FIG. 8. Dipole strength functions for ^{208}Pb deduced from the present (γ, γ') data (red circles), from $(^3\mathrm{He}, ^3\mathrm{He}')$ data (blue squares) [48], and from (p, p') data (green triangles) [51]. Also shown is the Lorentz curve from RIPL (black dashed line).

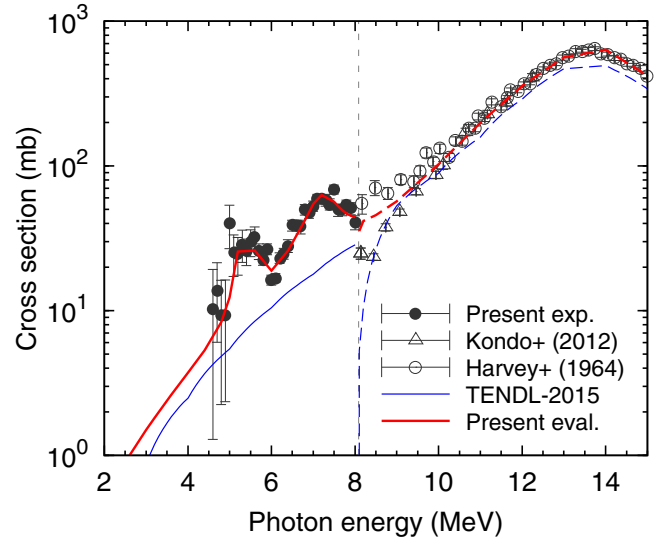

FIG. 9. Comparison of the calculated results for (γ, γ') reaction (thick solid line) and (γ, n) reaction (thick dashed line) with the measured data. The calculated data for photoabsorption and (γ, n) reaction cross sections are separated below and above the neutron separation energy of ^{206}Pb by a vertical dotted line. For comparison, the cross sections in TENDL-2015 are depicted by thin lines. It should be noted that the data of Harvey *et al.* [44] were multiplied by 1.22 following the suggestion in Ref. [62].

the $(^3\mathrm{He}, ^3\mathrm{He}')$ data may have various reasons. In ^{208}Pb, the structure of all three strength functions looks similar, but also in this case the magnitudes differ. Around the 5.5-MeV peak, the (p, p') data lie between the other two sets and in the region between 6 MeV and S_n the values of the three sets are almost equal.

The validity of the Brink-Axel hypothesis was recently proven for the case of ^{96}Mo on the basis of a comparison of new (p, p') data [53] with existing $(^3\mathrm{He}, ^3\mathrm{He}')$ data [54] and (γ, γ') data [32]. Similarly to the present cases of ^{206}Pb and ^{208}Pb, the $(^3\mathrm{He}, ^3\mathrm{He}')$ data are close to the (γ, γ') data between about 7.3 and 8.5 MeV but drop rapidly toward low energy. The (p, p') values lie between the ones of the other two sets and overlap with most of them within their uncertainties up to S_n. This agreement of the strength functions deduced from the three experiments serves as a proof of the Brink-Axel hypothesis. In fact, the simulation of γ-ray cascades performed in Ref. [32] and in the present work (see Sec. III B) is based on identical strength functions for excitation and deexcitation, i.e., on the Brink-Axel hypothesis. However, the authors of Ref. [53] state that an apparent violation of the Brink-Axel hypothesis was suggested by the (γ, γ') data in Ref. [32]. We note that there is neither such a statement in Ref. [32] nor does the just-mentioned compatibility of the data allow such a conclusion.

B. Evaluation of the neutron-capture cross section of ^{205}Pb

In order to evaluate the neutron-capture cross section of the unstable ^{205}Pb in the keV energy region, the present (γ, γ') data as well as existing (γ, n) data were used to constrain the PSF of ^{206}Pb. The cross sections of photon- and neutron-induced reactions were calculated by using the CCONE code [55], which is based on the Hauser-Feshbach statistical model with width fluctuation correction [56,57]. The neutron optical model was taken from Ref. [58]. The optical model potential (OMP) parameters of ^{205}Pb were the same as those of ^{206}Pb. The $E1$, $M1$, and $E2$ radiations were taken into account for γ-ray transitions. For the PSF of dominant $E1$ radiation, the modified Lorentzian model was adopted to calculate photon- and neutron-induced reaction cross sections [59]. The supplemental strength was taken into account by the standard Lorentzian model in order to reproduce two humps below the threshold energy of (γ, n) reaction. The PSFs for $M1$ and $E2$ radiations were employed according to the expression in Ref. [59]. The discrete excited levels were taken from the RIPL-3 database [41]. The adopted maximum energy of levels for ^{206}Pb was 3.279 MeV. Above the discrete levels the Gilbert-Cameron formalism [37] with the shell correction [60] was applied for the nuclear level density. It composes the constant temperature model for lower excitation energies and the Fermi-gas model for higher excitation energies [61].

The experimental data for the (γ, n) reaction were taken from Refs. [44,49]. The measured cross sections of (γ, n) and (γ, γ') reactions were used to determine model parameters such as resonance energies and width and peak cross sections expressing the GDR. The evaluated results of the measured data are shown in Fig. 9 which compares the calculated cross sections with the experimental data of (γ, n) and (γ, γ') reactions. It should be noted that Harvey *et al.* [44] measured one-neutron production cross sections which possibly include cross sections of the (γ, pn) and $(\gamma, \alpha n)$ reactions. However, their contributions are expected to be negligible in the present evaluation.

The calculated photoabsorption cross section is compared with the present (γ, γ') data below the photon energies of

TABLE II. GDR parameters of ^{206}Pb.

Energy (MeV)	Width (MeV)	Peak cross section (mb)
5.4	0.10	36.5
7.2	0.97	40.2
12.5	4.06	121.6
13.8	3.24	560.7

8.09 MeV in Fig. 9. The measured data show humps around about 5 and 7 MeV. In order to express the increase of the cross sections by a pygmylike resonance, a small contribution of $E1$ radiation was incorporated in the tail of GDR. The calculated result is consistent with the measured data as shown in Fig. 9. The GDR parameters needed to reproduce the measured cross sections were summarized in Table II. It is noted that there is a remarkable similarity of the peak in the cross section around about 5 MeV with that in ^{208}Pb [45,63]. In the shell-model calculations for ^{208}Pb this arises from two-particle two-hole excitations [45]. In Fig. 9, the (γ, n) and photoabsorption cross sections of TENDL-2015 were also represented for comparison. The (γ, n) reaction cross sections of TENDL-2015 are smaller than those of Harvey *et al.* [44] around the GDR peak. Its photoabsorption cross section is also smaller than the data derived in the present work.

The neutron-capture cross section was calculated by using the adopted PSF with the GDR parameters which were obtained by evaluating the photonuclear data. In Fig. 10, the result is illustrated together with the data of TENDL-2015 [64] and JEFF-3.2 [65]. These evaluated libraries have artificially generated neutron resonances. In the figure their cross sections were made groupwise in the resolved resonance region. TENDL-2015 and JEFF-3.2 have almost the same cross sections above 40 keV. The neutron-capture cross section obtained in the present work is close to those of TENDL-2015 and JEFF-3.2 above the resolved resonance region but is about 1.8 times larger than the results of previous work [28] in neutron energies between 10 and 10^3 keV. This discrepancy is possibly caused by the enhanced strength obtained in the analysis of the quasicontinuum as well as the difference of the level-density model used for ^{206}Pb.

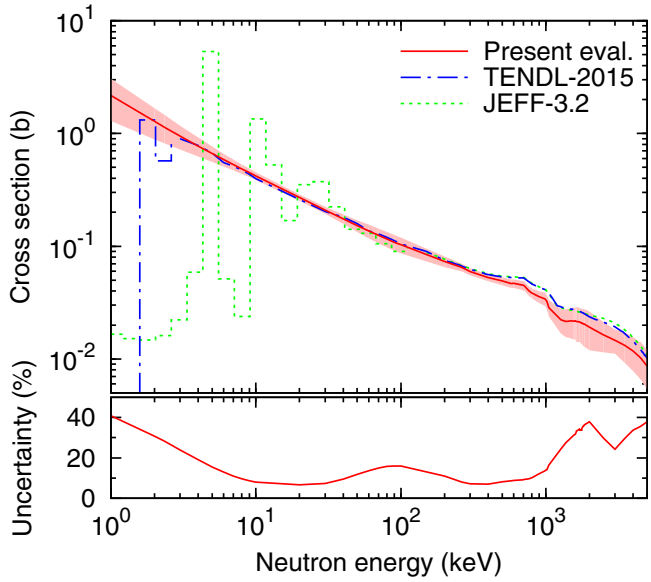

FIG. 10. Neutron-capture cross section of ^{205}Pb calculated by using the PSF deduced from the photonuclear data in the top panel. The deduced uncertainty is overlaid as a band around the cross section and presented in the bottom panel. The evaluated cross sections of TENDL-2015 (dot-dashed line) and JEFF-3.2 (dotted line) are also shown for comparison.

The uncertainty of the neutron-capture cross section for ^{205}Pb was estimated by the KALMAN code [66], which is based on the generalized least-squares method with Bayesian theorem. It was derived from an uncertainty propagation of measured (γ, n) and (γ, γ') reaction cross sections. The experimental uncertainties were used to constrain the parameter uncertainties of the reaction models in CCONE. The experimental data of Harvey *et al.* and Kondo *et al.* were adopted for the (γ, n) reaction. For the data of Kondo *et al.*, the systematic uncertainty of 4.4% was additionally taken into account from the literature [49] as its minimum estimation. The present data were used for the (γ, γ') reaction. In the covariance estimation the parameter covariance matrix was prepared as a prior one. The parameters of neutron OMP (potential radius, diffuseness and depth for real volume and imaginary surface terms for ^{205}Pb), level density (level-density parameters for ^{205,206}Pb), and PSF (resonance energies, widths, peak cross sections for the four resonances for ^{206}Pb) were considered as the matrix component. The sensitivities of the above parameters to the neutron-capture and photonuclear cross sections were calculated by CCONE. The cross section covariance matrix was finally obtained from the constrained parameter one with the parameter sensitivities. The resulting uncertainty of neutron-capture cross section is presented in Fig. 10. In the region between 10 and 10^3 keV the uncertainties are 6 to 16%, which are well constrained by the adopted experimental data. In contrast, the uncertainties are large above and below the energy region due to the uncertainties of level-density parameters for ^{206}Pb and neutron OMP parameters (potential radius and depth of real volume term).

Using the neutron-capture cross sections deduced above, we estimated the time variation of the ^{205}Pb amount produced in a typical subcritical reactor in the ADS [7,67]. We assumed neutron beam fluxes of 5×10^{14}, 5×10^{15}, and 5×10^{16} n/cm^2/s at a neutron energy of 100 keV around the Pb-Bi target position [67]. Figure 11 shows calculated fractions (in units of weight percent; wt%) of ^{205}Pb relative to initial amount of Pb materials as a function of the irradiation period. For a 10-year irradiation period, 0.01–0.4wt% of ^{205}Pb is produced. Since management of long-lived isotopes produced in a nuclear reactor is necessary for long-term sustenance of nuclear energy program, the accumulated amount of ^{205}Pb has to be evaluated as precisely as possible using a more realistic neutron flux in a lead-bismuth eutectic target [68].

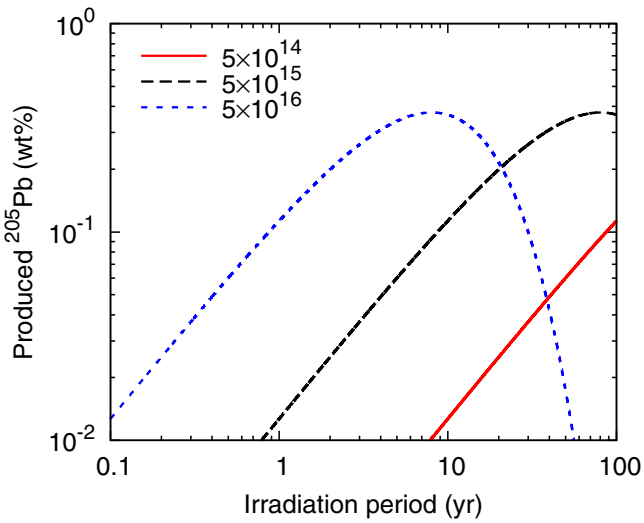

FIG. 11. Fractions (in units of weight percentage; wt%) of ^{205}Pb calculated for a typical subcritical reactor in ADS as a function of irradiation period with an assumption of neutron fluxes of 5×10^{14} (solid line), 5×10^{15} (dashed line), and 5×10^{16} (dotted line) n/cm^2/s.

V. CONCLUSION

The dipole strength distribution in ^{206}Pb up to the neutron separation energy has been studied in a photon-scattering experiment at the ELBE bremsstrahlung facility by using an electron beam at a kinetic energy of 10.5 MeV for the purpose of the evaluation of the neutron-capture cross sections for the unstable ^{205}Pb nucleus. We identified 85 $J = 1$ states and 3 $J = 2$ states below 8.2 MeV. The intensity distribution obtained from the measured spectra after a correction for detector response and a subtraction of atomic background in the target contains a quasicontinuum in addition to resolved peaks. Simulations of statistical γ-ray cascades have been performed to estimate the intensities of inelastic transitions and the branching ratios of the ground-state transitions. The photoabsorption cross section obtained in this way together with the (γ, n) cross-section data were compared with results of the calculations using the CCONE code. For the photon strength function of $E1$ radiation, the modified Lorentzian model was adopted. In the energy region around the maximum of the GDR, the results provide a good description for the (γ, n) cross sections. In the low-energy region below the neutron separation energy, the data obtained from the present (γ, γ') experiment was used to constrain the PSF. The neutron-capture cross sections of ^{205}Pb were calculated using the PSF fixed by the photonuclear data and compared with the evaluation of TENDL-2015 and JEFF-3.2. The neutron-capture cross section derived in this work is close to those of TENDL-2015 and JEFF-3.2 above the resolved resonance region.

ACKNOWLEDGMENTS

We thank the staff of the ELBE accelerator facility for cooperation during the experiments and A. Hartmann for the technical assistance. We also thank H. Ohgaki for providing the ^{206}Pb target and A. C. Larsen and M. Guttormsen for providing the (^{3}He, ^{3}He$'$) data and for valuable discussions. R.M. was supported by the U.S. Department of Energy, Office of Science, Office of Nuclear Physics, under Award No. DE-AC52-06NA25396. This work was supported in part by Grants-in-Aid for Scientific Research (C), No. 25400303 and No. 17K05482, from JSPS.

[1] M. Arnould, S. Goriely, and K. Takahashi, Phys. Rep. **450**, 97 (2007).
[2] M. B. Chadwick *et al.*, Nucl. Data Sheets **112**, 2887 (2011).
[3] M. Salvatores and G. Palmiotti, Prog. Part. Nucl. Phys. **66**, 144 (2011).
[4] S. Goriely, Phys. Lett. B **436**, 10 (1998).
[5] A. C. Larsen and S. Goriely, Phys. Rev. C **82**, 014318 (2010).
[6] H. Harada, NEA/WPEC-31, OECD, NEA/NSC/WPEC /DOC 446 (2014), https://www.oecd-nea.org/science/wpec/volume31/volume31.pdf.
[7] K. Nishihara, K. Iwanaga, K. Tsujimoto, Y. Kurata, H. Oigawa, and T. Iwasaki, J. Nucl. Sci. Tech. **45**, 812 (2008).
[8] S. Raman, J. B. McGrory, E. T. Jurney, and J. W. Starner, Phys. Rev. C **53**, 2732 (1996); **54**, 2786 (1996).
[9] A. Makinaga, R. Schwengner, G. Rusev, F. Dönau, S. Frauendorf, D. Bemmerer, R. Beyer, P. Crespo, M. Erhard, A. R. Junghans, J. Klug, K. Kosev, C. Nair, K. D. Schilling, and A. Wagner, Phys. Rev. C **82**, 024314 (2010).
[10] A. Makinaga, R. Massarczyk, R. Schwengner, M. Beard, F. Dönau, M. Anders, D. Bemmerer, R. Beyer, R. Hannaske, A. R. Junghans, M. Kempe, T. Kögler, M. Röder, K. Schmidt, and A. Wagner, Phys. Rev. C **90**, 044301 (2014).
[11] A. Makinaga, R. Massarczyk, M. Beard, R. Schwengner, H. Otsu, T. Al-Abdullah, M. Anders, D. Bemmerer, R. Hannaske, R. John, A. R. Junghans, S. E. Müller, M. Röder, K. Schmidt, and A. Wagner, Phys. Rev. C **94**, 044304 (2016).
[12] U. Kneissl, H. H. Pitz, and A. Zilges, Prog. Part. Nucl. Phys. **37**, 349 (1996); U. Kneissl, N. Pietralla, and A. Zilges, J. Phys. G **32**, R217(R) (2006).
[13] R. Schwengner, R. Beyer, F. Dönau, E. Grosse, A. Hartmann, A. R. Junghans, S. Mallion, G. Rusev, K. D. Schilling, W. Schulze, and A. Wagner, Nucl. Instrum. Methods A **555**, 211 (2005).
[14] R. Schwengner, G. Rusev, N. Benouaret, R. Beyer, M. Erhard, E. Grosse, A. R. Junghans, J. Klug, K. Kosev, L. Kostov, C. Nair, N. Nankov, K. D. Schilling, and A. Wagner, Phys. Rev. C **76**, 034321 (2007).
[15] G. Rusev, R. Schwengner, F. Dönau, M. Erhard, E. Grosse, A. R. Junghans, K. Kosev, K. D. Schilling, A. Wagner, F. Bečvář, and M. Krtička, Phys. Rev. C **77**, 064321 (2008).
[16] J. H. Kelley, E. Kwan, J. E. Purcell, C. G. Sheu, and H. R. Weller, Nucl. Phys. A **880**, 88 (2012).
[17] F. Metzger, in *Progress in Nuclear Physics*, edited by O. Frisch (Pergamon Press, New York, 1959), Vol. 7, pp. 53–88.
[18] S. Agostinelli *et al.*, Nucl. Instrum. Methods A **506**, 250 (2003).

[19] E. Haug, Radiat. Phys. Chem. **77**, 207 (2008).
[20] G. Roche, C. Ducos, and J. Proriol, Phys. Rev. A **5**, 2403 (1972).
[21] F. Salvat, J. D. Martinez, R. Mayol, and J. Parellada, Phys. Rev. A **36**, 467 (1987).
[22] G. Rusev, A. P. Tonchev, R. Schwengner, C. Sun, W. Tornow, and Y. K. Wu, Phys. Rev. C **79**, 047601 (2009).
[23] C. P. Swann, J. Franklin Inst. **298**, 321 (1974).
[24] D. F. Coope, L. E. Cannell, and M. K. Brussel, Phys. Rev. C **15**, 1977 (1977).
[25] T. Chapuran, R. Vodhanel, and M. K. Brussel, Phys. Rev. C **22**, 1420 (1980).
[26] J. Enders, P. von Brentano, J. Eberth, A. Fitzler, C. Fransen, R.-D. Herzberg, H. Kaiser, L. Käubler, P. von Neumann-Cosel, N. Pietralla, V. Yu. Ponomarev, A. Richter, R. Schwengner, and I. Wiedenhöver, Nucl. Phys. A **724**, 243 (2003).
[27] M. Schanz, A. Richter, and E. Lipparini, Phys. Rev. C **36**, 555 (1987).
[28] A. P. Tonchev, N. Tsoneva, C. Bhatia, C. W. Arnold, S. Goriely, S. L. Hammond, J. H. Kelley, H. Lenske, J. Piekarewicz, R. Raut, G. Rusev, T. Shizuma, and W. Tornow, Phys. Lett. B **773**, 20 (2017).
[29] R. Massarczyk, R. Schwengner, F. Dönau, E. Litvinova, G. Rusev, R. Beyer, R. Hannaske, A. R. Junghans, M. Kempe, J. H. Kelley, T. Kögler, K. Kosev, E. Kwan, M. Marta, A. Matic, C. Nair, R. Raut, K. D. Schilling, G. Schramm, D. Stach, A. P. Tonchev, W. Tornow, E. Trompler, A. Wagner, and D. Yakorev, Phys. Rev. C **86**, 014319 (2012).
[30] E. Trompler, Diploma thesis, Technische Universität Dresden 2009, Report FZD-523.
[31] S. Carson, C. Iliadis, J. Cesaratto, A. Champagne, L. Downen, M. Ivanovic, J. Kelley, R. Longland, J. R. Newton, G. Rusev, and A. P. Tonchev, Nucl. Instrum. Method A **618**, 190 (2010).
[32] G. Rusev, R. Schwengner, R. Beyer, M. Erhard, E. Grosse, A. R. Junghans, K. Kosev, C. Nair, K. D. Schilling, A. Wagner, F. Dönau, and S. Frauendorf, Phys. Rev. C **79**, 061302(R) (2009).
[33] G. Schramm, R. Massarczyk, A. R. Junghans, T. Belgya, R. Beyer, E. Birgersson, E. Grosse, M. Kempe, Z. Kis, K. Kosev, M. Krtička, A. Matic, K. D. Schilling, R. Schwengner, L. Szentmiklosi, A. Wagner, and J. L. Weil, Phys. Rev. C **85**, 014311 (2012).
[34] R. Massarczyk, R. Schwengner, F. Dönau, S. Frauendorf, M. Anders, D. Bemmerer, R. Beyer, C. Bhatia, E. Birgersson, M. Butterling, Z. Elekes, A. Ferrari, M. E. Gooden, R. Hannaske, A. R. Junghans, M. Kempe, J. H. Kelley, T. Kögler, A. Matic, M. L. Menzel, S. Müller, T. P. Reinhardt, M. Röder, G. Rusev, K. D. Schilling, K. Schmidt, G. Schramm, A. P. Tonchev, and W. Tornow, A. Wagner, Phys. Rev. Lett. **112**, 072501 (2014).
[35] F. Bečvář, Nucl. Instrum. Methods A **417**, 434 (1998).
[36] C. E. Porter and R. G. Thomas, Phys. Rev. **104**, 483 (1956).
[37] A. Gilbert and A. G. W. Cameron, Can. J. Phys. **43**, 1446 (1965).
[38] T. von Egidy and D. Bucurescu, Phys. Rev. C **80**, 054310 (2009).
[39] S. I. Al-Quraishi, S. M. Grimes, T. N. Massey, and D. A. Resler, Phys. Rev. C **67**, 015803 (2003).
[40] A. R. Junghans, G. Rusev, R. Schwengner, A. Wagner, and E. Grosse, Phys. Lett. B **670**, 200 (2008).
[41] R. Capote, M. Herman, P. Oblozinsky, P. G. Young, S. Goriely, T. Belgya, A. V. Ignatyuk, A. J. Koning, S. Hilaire, V. A. Plujko, M. Avrigeanu, O. Bersillon, M. B. Chadwick, T. Fukahori, Z. Ge, Y. Han, S. Kailas, J. Kopecky, V. M. Maslov, G. Reffo, M. Sin, E. Sh. Soukhovitskii, and P. Talou, Nucl. Data Sheets **110**, 3107 (2009).
[42] N. Benouaret, R. Schwengner, G. Rusev, F. Dönau, R. Beyer, M. Erhard, E. Grosse, A. R. Junghans, K. Kosev, C. Nair, K. D. Schilling, A. Wagner, and N. Bendjaballah, Phys. Rev. C **79**, 014303 (2009).
[43] R. Schwengner, R. Massarczyk, G. Rusev, N. Tsoneva, D. Bemmerer, R. Beyer, R. Hannaske, A. R. Junghans, J. H. Kelley, E. Kwan, H. Lenske, M. Marta, R. Raut, K. D. Schilling, A. Tonchev, W. Tornow, and A. Wagner, Phys. Rev. C **87**, 024306 (2013).
[44] R. R. Harvey, J. T. Caldwell, R. L. Bramblett, and S. C. Fultz, Phys. Rev. **136**, B126 (1964).
[45] R. Schwengner, R. Massarczyk, B. A. Brown, R. Beyer, F. Dönau, M. Erhard, E. Grosse, A. R. Junghans, K. Kosev, C. Nair, G. Rusev, K. D. Schilling, and A. Wagner, Phys. Rev. C **81**, 054315 (2010).
[46] R. Schwengner, G. Rusev, N. Tsoneva, N. Benouaret, R. Beyer, M. Erhard, E. Grosse, A. R. Junghans, J. Klug, K. Kösev, H. Lenske, C. Nair, K. D. Schilling, and A. Wagner, Phys. Rev. C **78**, 064314 (2008).
[47] N. U. H. Syed, M. Guttormsen, F. Ingebretsen, A. C. Larsen, T. Lönnroth, J. Rekstad, A. Schiller, S. Siem, and A. Voinov, Phys. Rev. C **79**, 024316 (2009).
[48] A. C. Larsen and M. Guttormsen (private communication).
[49] T. Kondo, H. Utsunomiya, S. Goriely, I. Daoutidis, C. Iwamoto, H. Akimune, A. Okamoto, T. Yamagata, M. Kamata, O. Itoh, H. Toyokawa, Y.-W. Lui, H. Harada, F. Kitatani, S. Hilaire, and A. J. Koning, Phys. Rev. C **86**, 014316 (2012).
[50] A. Veyssière, H. Beil, R. Bergère, P. Carlos, and A. Leprêtre, Nucl. Phys. A **159**, 561 (1970).
[51] S. Bassauer, P. von Neumann-Cosel, and A. Tamii, Phys. Rev. C **94**, 054313 (2016).
[52] D. M. Brink, doctoral thesis, Oxford University, 1955 (unpublished).
[53] D. Martin, P.von Neumann-Cosel, A. Tamii, N. Aoi, S. Bassauer, C. A. Bertulani, J. Carter, L. Donaldson, H. Fujita, Y. Fujita, T. Hashimoto, K. Hatanaka, T. Ito, A. Krugmann, B. Liu, Y. Maeda, K. Miki, R. Neveling, N. Pietralla, I. Poltoratska, V. Yu. Ponomarev, A. Richter, T. Shima, T. Yamamoto, and M. Zweidinger, Phys. Rev. Lett. **119**, 182503 (2017).
[54] M. Guttormsen, R. Chankova, U. Agvaanluvsan, E. Algin, L. A. Bernstein, F. Ingebretsen, T. Lönnroth, S. Messelt, G. E. Mitchell, J. Rekstad, A. Schiller, S. Siem, A. C. Sunde, A. Voinov, and S. Ødegard, Phys. Rev. C **71**, 044307 (2005).
[55] O. Iwamoto, N. Iwamoto, S. Kunieda, F. Minato, and K. Shibata, Nucl. Data Sheets **131**, 259 (2016).
[56] H. Gruppelaar and G. Reffo, Nucl. Sci. Eng. **62**, 756 (1977).
[57] P. A. Moldauer, Nucl. Phys. A **344**, 185 (1980).
[58] A. J. Koning, M. C. Duijvestijn, S. C. van der Marck, R. Klein Meulekamp, and A. Hogenbirk, Nucl. Sci. Eng. **156**, 357 (2007).
[59] J. Kopecky and M. Uhl, Phys. Rev. C **41**, 1941 (1990).
[60] A. V. Ignatyuk, G. N. Smirenkin, and A. S. Tishin, Yad. Fiz. **21**, 485 (1975) [Sov. J. Nucl. Phys. **21**, 255 (1975)].
[61] A. Mengoni and Y. Nakajima, J. Nucl. Sci. Technol. **31**, 151 (1994).
[62] B. L. Berman, R. E. Pywell, S. S. Dietrich, M. N. Thompson, K. G. McNeill, and J. W. Jury, Phys. Rev. C **36**, 1286 (1987).

[63] T. Shizuma, T. Hayakawa, H. Ohgaki, H. Toyokawa, T. Komatsubara, N. Kikuzawa, A. Tamii, and H. Nakada, Phys. Rev. C **78**, 061303(R) (2008).

[64] A. J. Koning, D. Rochman, J. Kopecky, J. Ch. Sublet, E. Bauge, S. Hilaire, P. Romain, B. Morillon, H. Duarte, S. van der Marck, S. Pomp, H. Sjostrand, R. Forrest, H. Henriksson, O. Cabellos, S. Goriely, J. Leppanen, H. Leeb, A. Plompen, and R. Mills, https://tendl.web.psi.ch/tendl_2015/tendl2015.html (2016).

[65] OECD Nuclear Energy Agency Data Bank, http://www.oecd-nea.org/dbforms/data/eva/evatapes/jeff_32/

[66] T. Kawano, K. Shibata, JAERI-Data/Code 97-037 (Japan Atomic Energy Agency) (1997) [in Japanease].

[67] H. Iwamoto, K. Nishihara, Y. Iwamoto, S. Hashimoto, N. Matsuda, T. Sato, M. Harada, and F. Maekawa, J. Nucl. Sci. Tech. **53**, 1585 (2016).

[68] T. Sugawara, K. Nishihara, H. Iwamoto, A. Oizumi, and K. Tsujimoto, J. Nucl. Sci. Tech. **53**, 2018 (2016).